Available online at www.sciencedirect.com

ScienceDirect

Procedia Manufacturing 47 (2020) 505–510

Procedia MANUFACTURING

www.elsevier.com/locate/procedia

23rd International Conference on Material Forming (ESAFORM 2020)

Effect of AM-induced Anisotropy on the Surface Integrity of Laser Powder Bed Fused Ti6Al4V Machined Parts

Lucia Lizzul[a,*], Rachele Bertolini[a], Andrea Ghiotti[a], Stefania Bruschi[a]

[a]*Department of Industrial Engineering, University of Padova, Via Venezia 1, 35131, Padova, Italy*

* Corresponding author. Tel.: +39 49-827 6819. *E-mail address:* lucia.lizzul@phd.unipd.it

Abstract

Additive Manufacturing processes lead to microstructural anisotropy of the parts, mainly as a consequence of the build-up orientation and sample height, since each layer experiences different thermal histories from the bottom to the top of the part. Such induced anisotropy generally remains after the heat treatment and may influence the performances of the cutting processes that are usually performed to finish the part functional surfaces. In this paper, the surface integrity of machined laser powder bed fused Ti6Al4V parts is analyzed in order to evaluate the effect of the build-up direction. To this aim, two different cutting processes, namely longitudinal and face turning, and cooling conditions, namely flood and cryogenic, were applied to parts obtained with different parameters of the additive manufacturing process. A wide surface and subsurface characterization was conducted, based on metallurgical, mechanical and topographical analyses. The results show that the additive manufacturing-induced anisotropy has a great influence on the machined surface integrity.

Keywords: Titanium; Surface integrity; Turning; Additive manufacturing

1. Introduction

Additive Manufactured (AM) metals constitute a material category that has aroused widespread interest in the industrial field, but a comprehensive knowledge of their behaviour and performances is yet to be fully gained [1]. In particular, the integration of the AM technology within the part process chain still represents a weak point due to the peculiar microstructure induced by AM that reflects on the part subsequent workability and in-service performances [2,3]. The AM process induces, in fact, a microstructural anisotropy of the part, since each deposited layer experiences different thermal histories. This is mainly dependent form the sample height and build-up orientation, because of the different cooling rates from the bottom to the top of the part, influenced also by the specific support structure [4]. Such anisotropy generally remains after the heat treatment [5,6], and may influence the performances of the cutting processes that are usually performed to finish the functional surfaces. This work investigates the effect of the AM strategy on the surface integrity of heat treated and machined Laser Powder Bed Fused (LPBF) Ti6Al4V parts. To this aim, both longitudinal and face semi-finishing turning operations were conducted on two LPBF Ti6Al4V bars obtained with different scanning strategies. Since cryogenic machining was demonstrated to be an effective way to improve surface integrity of machined parts [7,8], especially in the case of difficult-to-cut alloys like titanium ones, its effect was assessed in parallel to the flood one. The machined surfaces and subsurface were analyzed in terms of microstructural characteristics, micro and nanohardness, surface topography and defects. The results show that the AM-induced anisotropy plays a great role in determining the surface integrity of the machined workpiece, particularly as regards the surface roughness. The obtained results can be useful to better understand the AM parts machinability and improve their surface quality.

10.1016/j.promfg.2020.04.149

2. Experimental

2.1. Material

To manufacture the LPBF Ti6Al4V (grade 5) cylindrical bars of 25 mm of diameter and 60 mm of height, the EOS™ EOSINT M 280 was utilized. Two different scanning strategies were adopted, namely the stripes and the island ones. In the first case, a rotation of the scan vector of 67° on the next layer was used, with stripes width equal to 5 mm. For the second scanning strategy, square islands with 5 mm side were overlapped by 0.04 mm and shifted by 2.5 mm in both the X and Y directions. The laser power and the scanning speed were kept constant at 280 W and at 1200 mm/s, respectively, as well as the hatch spacing and layer thickness, set to 100 µm and 30 µm, respectively. The AM bars were subsequently heat treated in a protective argon atmosphere at 950°C for 30 min followed by furnace cooling using a Carbolite Gero™ RHF laboratory furnace. The heat treatment is generally recommended for AM parts to reduce residual stresses and improve mechanical properties by stabilizing their metastable microstructure and closing the porosities [5]. The latter was assessed trough density measurements using the Archimedes' method before and after the heat treatment. The samples were measured to be fully dense (density above 99.9% ± 0.2%), even before the heat treatment.

2.2. Machining trials

The Mori Seiki™ NL 1500 CNC lathe, equipped with a specially designed equipment for delivery of liquid nitrogen [9], was utilized for the machining tests. The CNMG120404-SM 1105 cutting tool insert by Sandvik-Coromant™ was utilized and a new cutting edge was employed for each cutting trial to prevent the influence of the tool wear. In order to evaluate the material anisotropy effect on the machinability, both semi-finishing longitudinal and face turning were carried out on 10 mm at the top of the AM bars. A roughing was first performed with two passes of 0.5 mm of depth of cut and 0.2 mm of feed rate at 80 m/min of cutting speed for both the turning operations. The following process parameters were used for the semi-finishing operations: 0.15 mm for both the depth of cut and feed rate with a cutting speed of 80 m/min. Turning tests were performed under flood and cryogenic cooling conditions. In flood condition the semi-synthetic cutting fluid Monroe™ Astro-Cut HD XBP mixed with water (1:20 mixing ratio) was utilized. For cryogenic machining operation the liquid nitrogen was used as coolant, which was sprayed against the tool rake and flank faces at a constant pressure of 15 bars. Fig. 1 shows the experimental plan and the code that is utilized to identify the different samples. Each operation was carried out three times and the average values of all the analyzed data reported with the related standard deviation.

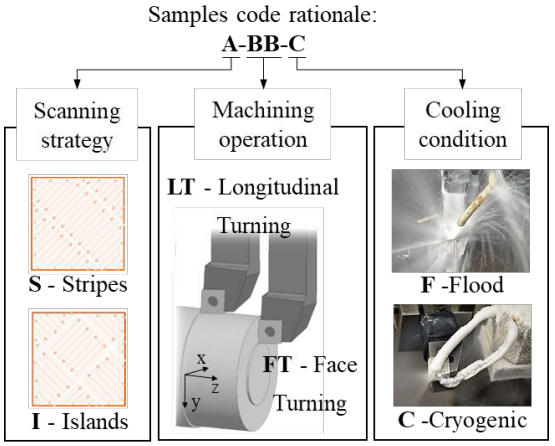

Fig. 1. Experimental plan and samples codes rationale.

2.3. Microstructural and mechanical characterization

To inspect their microstructure, the LPBF Ti6Al4V samples were carefully sectioned at the same height and hot mounted. After grinding using up to 4000 grit SiC paper, and polishing using colloidal silica dispersion in 3 wt% hydrogen peroxide, the metallographically prepared samples were cleaned and finally dried. To reveal grain boundaries, the Kroll's solution was used as etchant. Because of the different cutting directions of the two turning operations, two cross-sections were always evaluated in the metallographic examination. The effect of the face turning was assessed on the side view, which is parallel to the build-up direction, at 2 mm from the external diameter of the bars, whilst that of the longitudinal turning on the top view, which is perpendicular to the build-up direction. Micrographs were taken using a high definition digital camera of the Leica™ DMRE optical microscope. The β grains widths were measured on six different side view micrographs at 50× of magnification using the ASTM E112 line intercept method [10] via the Matlab™ software. Ten micrographs at 1000× of magnification were used to measure the extent of the plastically deformed lamellae, namely the Highly Deformed Layer (HDL), every 10 µm via the ImageJ™ software. Vickers microhardness measurements were carried out using the Leitz™ Durimet microhardness tester with a load of 50 g following the ASTM E92-17 standard [11]. Bulk microhardness was tested in all the material cross-sections through thirty unevenly distributed indentations for each condition. To assess the material strain hardening related to the lamellae deformation under the cutting forces, the nanohardness up to 20 µm of depth from the machined surface was measured using a Berkovich tip of the iMicro™ nanoindenter from Nanomechanics Inc. Three 4×5 matrices of nanoindentations were performed in different sub-superficial zones. The indentations were spaced 5 µm apart from each other and the load was set equal to 30 mN. Nanohardness analysis was performed as well on the specimen bulk by making three 4×4 matrices randomly distributed on all the examined cross-sections. All the above-mentioned measurements were recorded to calculate the average values and the respective standard deviations.

2.4. Surface finishing analysis

The machined surfaces were scanned using the Sensofar™ PLU-Neox optical profiler with a 20x Nikon™ confocal objective. Data processing, filtering and evaluation of the surface texture parameters were performed according to the ISO 25178 series [12]. Machined surfaces present a texture that strongly influences their in-service performances [13]. The most noteworthy roughness parameters to describe surface performances in terms of surface topography were taken into consideration, i.e. the arithmetical mean height (*Sa*), the skewness of the scale-limited surface (*Ssk*), the reduced valley depth (*Svk*), and the peak height (*Spk*). The *Sa* parameter is the most common areal parameter, which constitutes a reference for comparison with other research data; *Ssk* refers to the symmetry of the profile about the mean line and is useful to describe the load carrying ability of a surface and its corrosion tendency. *Svk* is a functional parameter that denotes the valley depth below the core roughness, useful to discriminate the presence of possible stress concentration sites or dales where a substance (a lubricant or a corrosive fluid) can accumulate. The other functional parameter is *Spk*, which represents the mean height of peaks above the core surface that are surface sites prone to corrosion and material which is likely to be removed during in rubbing surfaces.

Finally, the FEI™ QUANTA 450 Scanning Electron Microscope (SEM) with the Backscattered Electron Detector (BSED) was utilized to evaluate the presence of defects on the machined surfaces.

3. Results

3.1. LPBF microstructural characteristics

Fig. 2 shows the typical microstructure along the Build-up Direction (BD) of the heat-treated LPBF Ti6Al4V. Elongated prior β grains developed along the BD, i.e. along the Z axis, with continuous α phase layers at their boundaries, shown by the red arrows in the figure. Inside the prior β grains an α (in light) and β (in dark) phases mixture was found. The different scanning strategy led to different β grains width as shown in the micrographs and the size distribution histograms of Fig. 3. The bars manufactured with the stripes scanning strategy (Fig. 3 (a)) showed a β grains width 44% higher than the one of the bars manufactured with the islands scanning strategy (Fig. 3 (b)).

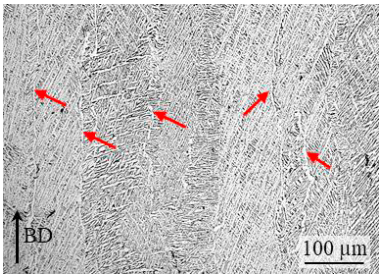

Fig. 2. Microstructure along the BD of the heat-treated LPBF Ti6Al4V. Red arrows show the continuous α phase layers along the prior β grains boundaries.

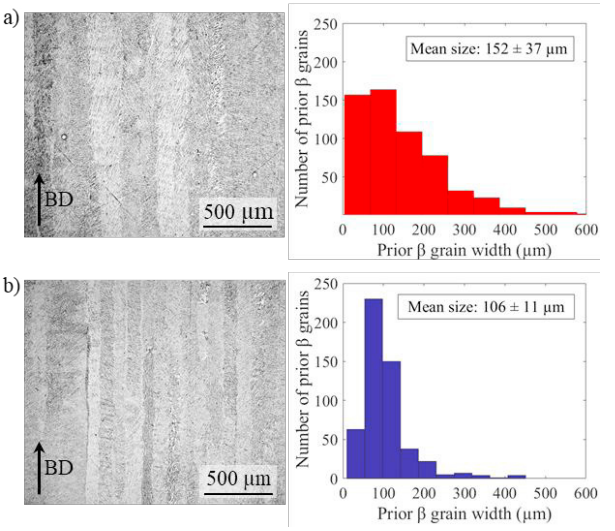

Fig. 3. Micrographs along the BD and size distribution histograms of the prior β grains width and their mean size for the LPBF bars with stripes scanning strategy (a) and island scanning strategy (b).

The microhardness values of the surfaces along the BD of the two LPBF bars are reported in Table 1. The LPBF Ti6Al4V bars obtained with the stripes scanning strategy resulted to have a 17% lower microhardness compared to the bars obtained with the islands strategy.

Table 1. Microhardness of the LPBF Ti6Al4V surfaces along the BD.

Scanning strategy	HV0.05
Stripes	307 ± 14
Islands	359 ± 18

3.2. Microstructural and mechanical alterations upon machining

For what concerns the extent of the lamellae deformed under the cutting forces, longitudinal turning led to lower HDL thicknesses with respect to face turning, as reported in Fig. 4. This was evident for the S-F and S-C samples, while for the I-F and I-C ones the trend was maintained even if the difference between the extension of the HDLs of the two turning operations was much less. Overall, flood turning led to higher HDL thicknesses than cryogenic one. Anyway, considering the

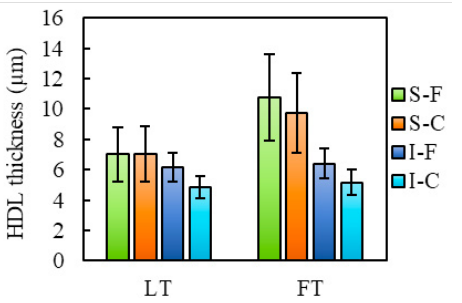

Fig. 4. HDL thickness of the machined subsurface.

standard deviation, the differences between the two cooling conditions when machining the bars manufactured with the stripes scanning strategy were not substantial, leading to comparable HDLs. A more evident difference was found in the samples from the bars manufactured with the islands scanning strategy.

The nanohardness percentage variation of the sample machined subsurface referring to the bulk nanohardness was measured and the results reported in Fig. 5. It is possible to observe that the nanohardness variation of the machined subsurface was generally lower for the face turned samples compared to the longitudinal turned ones. At the same way, the bars obtained with the island scanning strategy showed a lower strain hardening compared to the ones manufactured with the stripes pattern. The S-FT-C sample showed an own trend, being its strain hardening far higher compared to the other face turned bars.

3.3. Surface alterations upon machining

Fig. 6 reports the *Sa* values for all the machined surfaces. Overall, the samples manufactured with the islands pattern allowed for surfaces with lower surface roughness compared to the samples manufactured with the stripes one. The same trend was found between the face turned samples compared to longitudinal machined ones. In particular, a great reduction of *Sa* values was noted when machining in cryogenic conditions rather than in flood ones. In fact, the *Sa* values of the S-FT-F and I-FT-F samples were respectively 80% and 40% higher than the S-FT-C and I-FT-C ones. The face turning operation led to the formation of a double peak that was more pronounced in cryogenic cooling conditions compared to the flood ones.

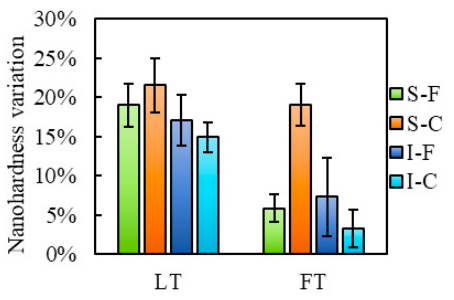

Fig. 5. Nanohardness percentage variation of the machined subsurface.

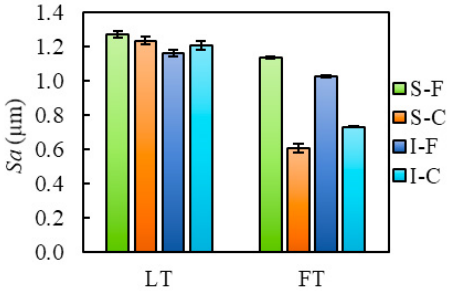

Fig. 6. Surface roughness of the machined surfaces.

In terms of functional surface texture parameters, reported in Table 2, this corresponded to lower *Spk* and higher *Svk* values. These surfaces presented the height distribution averagely skewed below the mean plane (*Ssk* values set in the middle). On the contrary, longitudinal turning produced profiles with marked peaks that were more pronounced in cryogenic turned samples. These specimens, in fact, reported the highest *Spk* values. At the same time, these surfaces were the most skewed below the mean plane (highest *Ssk* values) even if with highest peaks. This result is a consequence of the fact that the peaks are spiked and the material principally distributed below the mean plane.

Table 2. Functional surface texture parameters of the machined surfaces.

Sample	Ssk	Spk (µm)	Svk (µm)
S-LT-F	0.16 ± 0.02	0.77 ± 0.04	0.19 ± 0.03
S-FT-F	0.27 ± 0.02	1.13 ± 0.04	0.20 ± 0.02
S-LT-C	0.66 ± 0.04	2.45 ± 0.03	0.24 ± 0.02
S-FT-C	0.39 ± 0.02	0.16 ± 0.02	0.62 ± 0.02
I-LT-F	0.10 ± 0.03	0.57 ± 0.11	0.42 ± 0.26
I-FT-F	0.14 ± 0.02	0.93 ± 0.09	0.18 ± 0.03
I-LT-C	0.65 ± 0.01	2.21 ± 0.05	0.24 ± 0.05
I-FT-C	0.34 ± 0.03	0.14 ± 0.00	0.71 ± 0.08

Fig. 7 shows the defects of the machined surfaces. The surfaces were characterized by the typical defects found when machining difficult-to-cut alloys such as is the titanium alloy Ti4Al4V [14,15]. Between the longitudinal and face turned surfaces, there were no major differences apart from greater tearing in the longitudinal turned surfaces, which was accentuated in cryogenic machining. Furthermore, the type of scanning strategy had no observable influence on the occurrence of surface defects. The main differences were found between the two types of cooling conditions. In fact, in flood conditions, the surfaces reported higher amount of adhered material and smeared feed marks than the cryogenic turned surfaces.

4. Discussion

The microstructure described in § 3.1 shows a material marked anisotropy, which differed depending on the scanning strategy utilized to manufacture the LPBF samples. This microstructural anisotropy influenced the material response to the machining process. Thereafter, the effect of the material anisotropy, cutting direction and cooling conditions on the alloy machinability is discussed in detail.

4.1. Influence of the material anisotropy on the machined surface integrity

The different β grains size of the examined samples showed in Fig. 3 is related to the different thermal history that the fused powder layers experienced. In fact, the lower the cooling rate the wider the β grains [4]. With the stripes scanning strategy the deposited material remained at higher temperatures for a

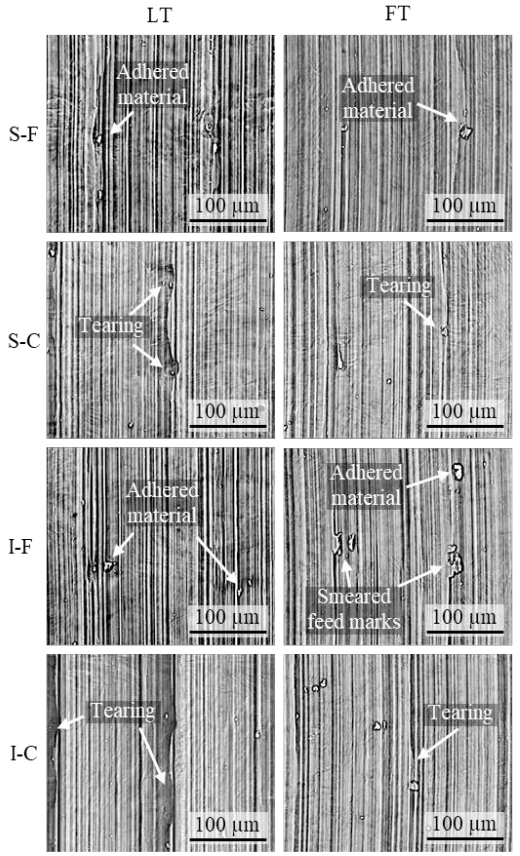

Fig. 7. Machined surface defects.

longer time compared to what happened using the island scanning strategy. The cooling rate influenced in the same way also the α lamellae thickness that plays a role in determining the microhardness of the alloy accordingly to the Hall-Petch equation. The microhardness values measured in this work resulted to be inversely proportional to the β grains size in accordance to what found by Sharma et al. [4]. In fact, the wider the β grains the thicker the α lamellae and the lower the microhardness.

The higher microhardness of the island scanned samples compared to the stripes scanned ones led to a lower extent of the deformed lamellae, thus to a lower HDL thickness as shown in Fig. 4. For the same reason, also the nanohardness variation of the machined subsurface was generally lower for the island scanned samples as reported in Fig. 5. Özel at al. [16] demonstrated that harder surfaces led to higher values of surface roughness in turning. This was not verified in the examined samples because of the influence of the peculiar LPBF microstructure. Literature studies where the mechanical behavior of AM Ti6Al4V titanium alloy was taken into consideration [2,3] showed that the fracture occurred in correspondence to the α phase layers that form along the β grains boundaries upon heat treatment. The α phase layers represent a material discontinuity that weakens the material integrity, and at the same time, may favor the material removal during cutting. According to this, the cutting forces needed to cut the island scanned samples, which showed the highest density of discontinuity layers because of the minor β grains width, should be lower and lead to machined surfaces with lower roughness [16]. This was verified as presented in § 3.3 where the *Sa* values for all the machined surfaces were reported. As for the other surface texture parameters taken into consideration and reported in Table 2, it was found that, in general, the island scanned samples reported lower *Spk* and *Ssk* values and higher *Svk* values, compared to the stripes scanned ones all conditions being equal. This means that the surfaces of the island scanning strategy allowed for machined surfaces with smaller peaks and deeper valleys.

4.2. Influence of the cutting direction on the machined surface integrity

During face turning the cutting insert cuts the material through the entire cross-sectional area of the cylindrical bar. This means that the cutting edge meets the weak α phase layers more frequently as if entering in contact with a material that shows less shear strength. This explains both the lower *Sa* values measured in face turning operations compared to the longitudinal turning ones and the greater variability of *Sa* values found in face turned samples. The main effect of the different cutting directions on the surface texture was, as mentioned in § 3.3, that the longitudinal turning led to single peaks roughness profiles, while the face one led to double peaks profiles. It was not possible to point out a defined trend to describe the variation of the functional roughness parameters with respect to the two cutting directions as the main differences were due to the different cooling conditions. On average, the longitudinal turning brought to surfaces with higher *Spk* and *Ssk* values and smaller *Svk* values, therefore to surfaces with high peaks and less deep valleys. On the basis of the same considerations made to explain the *Sa* results, the strain hardening (i.e. the nanohardness variation) of the machined subsurface was generally lower for face turned samples since the material showed less shear strength and less deformed lamellae. In determining the HDL thickness, the effect of the material microhardness played a more important role than the turning operation, since the HDL thickness was higher for face turned samples. In Fig. 8 the micrographs of the HDLs of two samples differing just for the turning operation are reported as example.

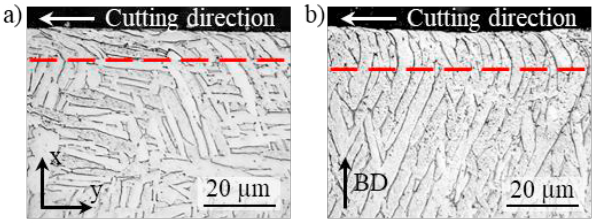

Fig. 8. HDL extent of a) S-LT-F and b) S-FT-F samples.

4.3. Influence of the cooling condition on the machined surface integrity

For what concerns the effect of the cooling condition on the surface roughness, cryogenic cooling allowed for lower *Sa*

values compared to flood machining. The main differences between the two cooling conditions were reported by the face turned samples, while for the longitudinal turned samples the differences were negligible. Thus, it can be stated that the cryogenic cooling highlighted the difference between the two cutting directions, an effect that was also found on the other surface texture parameters examined. In fact, the differences in such parameters values among the samples were minor when flood conditions were applied. This result can be related to the lower cutting temperature characterizing the cryogenic operations, which limits the material plastic deformation while cutting, enhancing the influence played by the α phase layers as previously described. As stated in § 4.2, in the face turned samples a double peak formed and the cryogenic conditions allowed for an intensification of this feature because of the low cutting temperatures that avoided the local softening of the material peaks. The same effect was found in longitudinal turned samples, whose marked peaks were more pronounced in cryogenic conditions, being this feature already found in previous works on AM Ti6Al4V cryogenic turning [7]. The cryogenic machining, compared to the flood one, led to a sharp increase in the mean height of the peaks (higher *Spk* values) in the case of longitudinal turned surfaces, while there was a decrease of this parameter in the face turned ones. The cryogenic cooling had a specular effect on the *Svk* parameter bringing to a sharp increase in the average depth of the valleys in the case of the face turned samples, while there was a decrease of these in the longitudinal turned ones. The surface defects analysis showed that the cryogenic machined surfaces were characterized by a higher amount of tearing, because of the low temperatures. The latter reduced at the same time the extend of the deformed lamellae (lower HDLs) in all the examined cases, even if the differences were not statistically significant, when considering the standard deviations as can be seen in Fig. 4. Cryogenic machining allowed for a higher strain hardening of the subsurface compared to the flood machining, only in the case of the samples manufactured with the stripes scanning strategy. This was particularly evident in the S-FT samples. This means, once again, that the cryogenic cooling highlights the material anisotropy.

5. Conclusions

In this work the effect of the peculiar AM-induced microstructure on machined surface integrity was assessed. Ti6Al4V cylindrical bars were additive manufactured using the LPBF technique by means of two different scanning strategies, namely stripes and islands. The bars were longitudinal and face turned afterwards under flood and cryogenic conditions. The results of the research point out the clear influence of the AM parameters on the microstructural anisotropy, which, in turns, influences the machined surface integrity. The effect of the different cutting directions and cooling conditions was also taken into consideration. The main results can be summarized as follows:

- The scanning strategy influenced the prior β grains size that is related to the material microhardness.
- The sample microhardness influenced the HDL thickness and the extent of the strain hardening of the machined subsurface of the different scanning strategy.
- The machined surface roughness was mostly influenced by the LPBF microstructure features, such as the α phase layers at the grain boundaries of the prior β grains.
- Cryogenic cooling allowed for a lower surface roughness and enhanced the effect of the material anisotropy in determining the surface integrity.

The results of this research can be useful to better understand the AM Ti6Al4V machinability and may represent a starting point for developing the analyses by varying the process and cutting parameters.

References

[1] Jiménez M, Romero L, Domínguez IA, Espinosa MDM, Domínguez M. Additive Manufacturing Technologies: An Overview about 3D Printing Methods and Future Prospects. Complexity 2019;2019.

[2] Carroll BE, Palmer TA, Beese AM. Anisotropic tensile behavior of Ti-6Al-4V components fabricated with directed energy deposition additive manufacturing. Acta Mater 2015;87:309–20.

[3] Simonelli M, Tse YY, Tuck C. Effect of the build orientation on the mechanical properties and fracture modes of SLM Ti-6Al-4V. Mater Sci Eng A 2014;616:1–11.

[4] Sharma H, Parfitt D, Syed AK, Wimpenny D, Muzangaza E, Baxter G, et al. A critical evaluation of the microstructural gradient along the build direction in electron beam melted Ti-6Al-4V alloy. Mater Sci Eng A 2019;744:182–94.

[5] Vrancken B, Thijs L, Kruth JP, Van Humbeeck J. Heat treatment of Ti6Al4V produced by Selective Laser Melting: Microstructure and mechanical properties. J Alloys Compd 2012;541:177–85.

[6] Liverani E, Toschi S, Ceschini L, Fortunato A. Effect of selective laser melting (SLM) process parameters on microstructure and mechanical properties of 316L austenitic stainless steel. J Mater Process Technol 2017;249:255–63.

[7] Bertolini R, Lizzul L, Pezzato L, Ghiotti A, Bruschi S. Improving surface integrity and corrosion resistance of additive manufactured Ti6Al4V alloy by cryogenic machining. Int J Adv Manuf Technol 2019;104:2839–50.

[8] Bruschi S, Bertolini R, Bordin A, Medea F, Ghiotti A. Influence of the machining parameters and cooling strategies on the wear behavior of wrought and additive manufactured Ti6Al4V for biomedical applications. Tribol Int 2016;102:133–42.

[9] Bordin A, Bruschi S, Ghiotti A, Bariani PF. Analysis of tool wear in cryogenic machining of additive manufactured Ti6Al4V alloy. Wear 2015;328–329:89–99.

[10] ASTM E112 - Standard Test Methods for Determining Average Grain Size 2013.

[11] ASTM E92: Standard Test Methods for Vickers Hardness and Knoop Hardness of Metallic Materials 2017.

[12] ISO 25178-1:Surface texture: Areal Part 1: Indication of surface texture 2016.

[13] Jawahir IS, Brinksmeier E, M'Saoubi R, Aspinwall DK, Outeiro JC, Meyer D, et al. Surface integrity in material removal processes: Recent advances. CIRP Ann - Manuf Technol 2011;60:603–26.

[14] Ezugwu EO, Bonney J, Da Silva RB, Çakir O. Surface integrity of finished turned Ti-6Al-4V alloy with PCD tools using conventional and high pressure coolant supplies. Int J Mach Tools Manuf 2007;47:884–91.

[15] Ulutan D, Ozel T. Machining induced surface integrity in titanium and nickel alloys : A review. Int J Mach Tools Manuf 2011;51:250–80.

[16] Özel T, Hsu TK, Zeren E. Effects of cutting edge geometry, workpiece hardness, feed rate and cutting speed on surface roughness and forces in finish turning of hardened AISI H13 steel. Int J Adv Manuf Technol 2005;25:262–9.